Dynamic Programming and Fuzzy Classification for the Automatic Segmentation of the Carotid in Ultrasound Images

Rui Rocha
INEB-Instituto de Engenharia Biomédica; ISEP-Instituto Superior de Engenharia do Porto
Campus da FEUP, Rua Dr. Roberto Frias, Edif. I - poente, 4200-465 Porto, Portugal
rhr@isep.ipp.pt

Jorge Silva
INEB-Instituto de Engenharia Biomédica; Universidade do Porto, Faculdade de Engenharia
jsilva@fe.up.pt

Aurélio Campilho
INEB-Instituto de Engenharia Biomédica; Universidade do Porto, Faculdade de Engenharia
campilho@fe.up.pt

Abstract

A new approach is proposed for the automatic detection of the near-end and far-end intima and adventitia inner boundaries in ultrasound images of the common carotid artery. This method uses the instantaneous coefficient of variation edge detector, fuzzy classification of edges, several discriminating features of the carotid wall boundaries and dynamic programming. The carotid wall boundaries are detected both in healthy and in atherosclerotic arteries, with a wide range of plaque types and sizes. Manual and automatic results are significantly better for the far-end wall, where the automatic detection shows an accuracy similar to manual detections. The application of this approach in clinical practice is encouraged by the results for the far-end wall and the short computation time.

1 Introduction

Atherosclerosis is a serious disease of the arteries that can lead to cardiovascular events like myocardial infarction and stroke. One of the most frequently used methods of diagnosis of this disease is the measurement of the intima-media thickness (IMT) of the carotid artery [1], the distance between the innermost boundaries of the intima and the adventitia layers of the artery wall.

The IMT measurement is often performed in B-mode ultrasound images due to their lower cost and smaller risk for the patient than alternative medical imaging modalities [2]. The common carotid artery (CCA) is often used in clinical practice because it is easier to segment than other regions, like the bifurcation of the artery.

Several techniques have been previously introduced for the detection of the carotid boundaries in ultrasound images, like [3–9]. However, all these techniques have important limitations, like the ones referred in [8]. This explains why the manual segmentation is still the most common procedure in clinical practice.

This paper introduces a new approach for the automatic detection of the inner boundaries of the intima and adventitia layers (represented by B_{int} and B_{adv} in Fig. 1) at the near-end (NE) and far-end (FE) artery walls in B-mode images of the CCA. As in [3], the proposed method also uses dynamic programming (DP), but it takes advantage of recent developments in edge detection in ultrasound images [10, 11], it requires the training of less parameters and it uses new discriminating features of the intima and the adventitia.

Recently, we have introduced in [8, 9] another approach to the same problem. This approach used RANSAC to find the best fit of a cubic spline to each adventitia inner boundary. A combination of dynamic programming, smooth intensity thresholding surfaces and geometric snakes was used to detect the intima.

This paper is focused on the description of the new approach and on some results that illustrate the improvements, when compared to [8] and [9], namely, more reliable segmentations of the FE wall and a shorter processing time.

2 Materials and methods

2.1 Image database

The image database is the one described in [8], consisting of 50 longitudinal B-mode images of the CCA, acquired with a Philips HDI 5000 ultrasound system and recorded with 256 gray levels. It refers to 25 different symptomatic patients, with several classes (classes II-IV), sizes and shapes of plaques [8]. The use of more than one image of the same patient increases the size of the database and allows the study of the inter-subject error that can result from differences in the contrast, in the speckle and in the visibility of the boundaries of the artery wall. However, the number of images taken from each patient should be small to minimize correlation between images.

The resolution was normalized to 0.09 mm, a common value used in clinical practice.

The manual segmentation of each image performed by a medical expert was used as the ground truth.

2.2 Description of the approach

The proposed approach can be summarized in four steps, described in the following subsections.

2.2.1 ROI Selection

The proposed approach begins with the selection of a region of interest (ROI) in a B-mode image of the CCA,

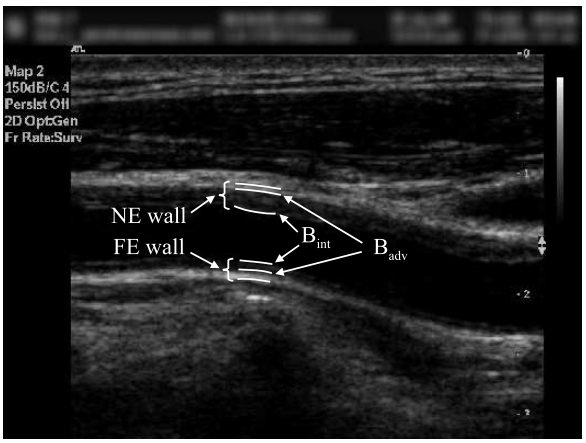

Figure 1. Example of a B-mode image of the CCA. At the NE and FE walls, the inner boundaries of the intima and of the adventitia are represented by B_{int} and B_{adv}, respectively.

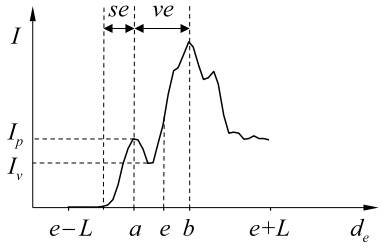

Figure 2. Example of a real intensity profile of a valley edge (segment ve), where: I is the intensity; e is the location of the edge; d_e is the distance from the edge in the direction of its intensity gradient, $\nabla I(e)$; a is the location of the lower maximum; b is the location of the higher maximum; and L is the maximum distance of search. Segment se corresponds to a step edge intensity profile.

like the one presented in Fig. 1, in order to remove the image borders with text or without any echo.

2.2.2 Fuzzy edge map and fuzzy valley edge map

This step consists of estimating two fuzzy edge maps that are fundamental for the detection of the carotid wall boundaries, namely the fuzzy step edge map ($f_{\mathrm{FM}}(x,y)$) and the fuzzy valley edge map ($f_{\mathrm{FVM}}(x,y)$).

The fuzzy step edge map is computed as in [8], using the instantaneous coefficient of variation (ICOV) edge detector [10,11]. The likelihood of the pixel at location (x,y) being an edge is represented by $f(x,y) = 1 - \tau(x,y)$, where $\tau(x,y)$ is the Tukey's function for the ICOV of this pixel, given by

$$\tau(x,y) = \begin{cases} \left[1 - \left(\frac{\mathrm{ICOV}(x,y)}{\sigma_s}\right)^2\right]^2 & \mathrm{ICOV} < \sigma_s \\ 0 & \mathrm{ICOV} \geq \sigma_s \end{cases} \quad (1)$$

where $\sigma_s = \sqrt{5}\sigma_e$ and σ_e is the image edge scale, estimated from the set of pixels with positive ICOV using robust statistics [8]. The fuzzy edge map, $f_{\mathrm{FM}}(x,y)$, is set equal to $f(x,y)$ at pixels that are local maxima of the ICOV and to zero at other pixels.

In healthy subjects, the intima and the adventitia appear as two almost parallel echogenic lines separated by a hypoechogenic media region, forming an intensity valley shaped edge (Fig. 2) known as the 'double line' pattern [12]. The determination of the fuzzy valley edge map is based on the search in the direction of the gradient, up to a certain distance L from the edge pixel, for an intensity profile like the one presented in Fig. 2. The fuzzy valley edge map is estimated by $f^*(x,y) = 1 - \tau^*(x,y)$, being $\tau^*(x,y)$ given by

$$\tau^*(x,y) = \begin{cases} \left[1 - \left(\frac{\Delta I(x,y)}{\sigma_s^*}\right)^2\right]^2 & \Delta I < \sigma_s^* \\ 0 & \Delta I \geq \sigma_s^* \end{cases} \quad (2)$$

where $\sigma_s^* = \sqrt{5}\sigma^*$ and σ^* is the scale for the normalized amplitude of the lower maxima, $\Delta I(x,y)$, defined as

$$\Delta I = (I_p - I_v)/(I_v + \epsilon) \quad (3)$$

where ϵ is a small positive constant used to avoid divisions by zero. $\Delta I(x,y)$ is estimated from the subset of fuzzy edge pixels for which $I_p > 0$. $f_{\mathrm{FVM}}(x,y)$ is set equal to $f^*(x,y)$ at the ICOV local maxima and to zero at other pixels.

2.2.3 Detection of the carotid intima

In this third step, the NE and the FE intima inner boundaries are estimated (Fig. 3).

To take advantage of *a priori* knowledge about the NE and FE intima edges, edge pixels in each column of the ROI are processed in pairs to compute a NE and a FE fuzzy intima score map, $f_{\mathrm{NE\_FIM}}(x,y)$ and $f_{\mathrm{FE\_FIM}}(x,y)$, shown in Fig. 3 a) and Fig. 3 b). Each pair of edge pixels has to satisfy two constraints: the intensity gradient points upward at the NE boundary and downward at the FE boundary; the distance between these two pixels is neither smaller than a minimum lumen[1] diameter, $\mathrm{LD_{min}}$, nor larger than a maximum carotid diameter, $\mathrm{CD_{max}}$. The maximum lumen diameter is approximately the same as $\mathrm{CD_{max}}$ since the IMT is very small in healthy people.

Taking into account that no edges are expected in the lumen, this property is embedded in a fuzzy score computed for each pair of plausible NE-FE intima edge pixels, given by

$$S_{\mathrm{I}} = e^{-z^2/2} \quad (4)$$

where: $z = \mathrm{FM_{max}}/\sigma_{\mathrm{FM}}$; $\mathrm{FM_{max}}$ is the maximum value of the fuzzy edge map between the two NE-FE intima edge pixels; σ_{FM} is a scale parameter. The maximum value of S_{I} found for each edge pixel of the pair is saved in $f_{\mathrm{NE\_FIM}}(x,y)$ and $f_{\mathrm{FE\_FIM}}(x,y)$.

The NE intima boundary (first white contour from the top in Fig. 3 c)) is estimated as a longitudinal smooth contour that maximizes a cumulative score, computed from $f_{\mathrm{NE\_FIM}}(x,y)$ and implemented as a gain function, G_{I}, with two terms: one embedding edge information derived from $f_{\mathrm{NE\_FIM}}(x,y)$ and the other conveying geometric smoothness information. G_{I}

[1] The lumen is the region inside the artery where the blood flows.

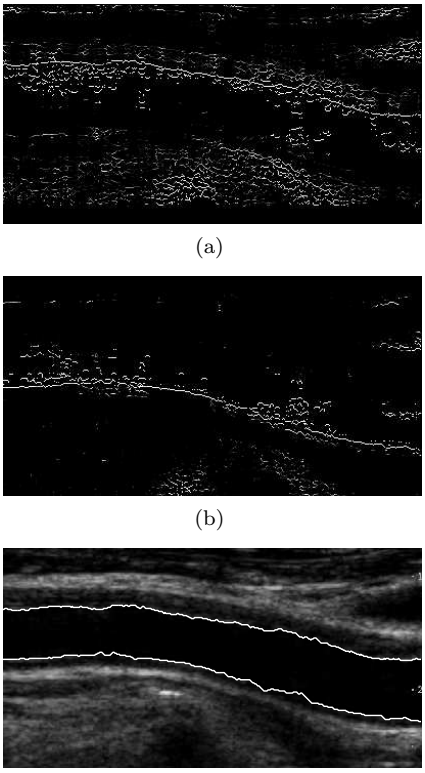

Figure 3. Detection of the intima inner boundary for a ROI in the image of Fig. 1: a) $f_{\text{NE\_FIM}}(x, y)$; b) $f_{\text{FE\_FIM}}(x, y)$; c) estimated intima inner boundary.

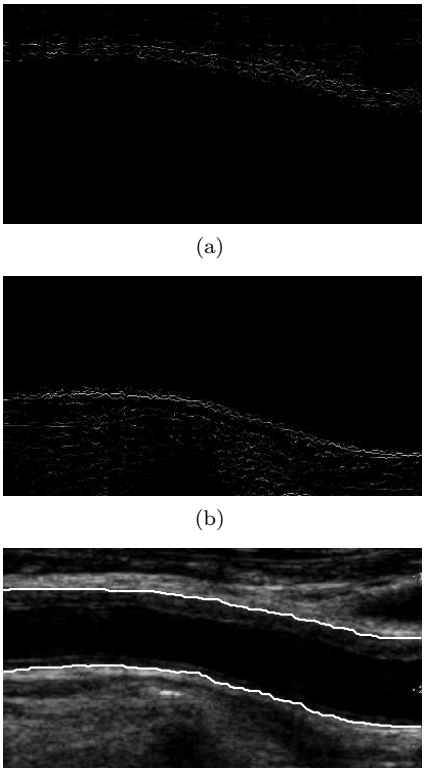

Figure 4. Detection of the adventitia inner boundary for a ROI in the image of Fig. 1: a) $f_{\text{NE\_FAM}}(x, y)$; b) $f_{\text{FE\_FAM}}(x, y)$; c) estimated adventitia inner boundary.

is given by

$$G_{\text{I}} = \psi(x_1, y_1) + \sum_{j=2}^{N} [\psi(x_j, y_j) + \lambda \rho(x_j, y_j)] \qquad (5)$$

where: N is the number of columns of the ROI; (x_j, y_j) are the coordinates of the contour pixel at column j; $\psi(x_j, y_j) = f_{\text{NE\_FIM}}(x_j, y_j)$; $\rho(x_j, y_j)$ is a geometric term with values $\rho(x_j, y_j) = 1$ if $y_j = y_{j-1}$ and $\rho(x_j, y_j) = 1/\sqrt{2}$ otherwise; λ is a weight parameter.

A similar procedure is used to estimate the FE intima boundary (second white contour from the top in Fig. 3 c)), by setting $\psi(x_j, y_j) = f_{\text{FE\_FIM}}(x_j, y_j)$.

2.2.4 Detection of the carotid adventitia

The last step of the method consists of the determination of the adventitia inner boundaries (Fig. 4).

In order to consider both step edges and valley edges, the fuzzy adventitia edge map is computed as $f_{\text{FAM}}(x, y) = (f_{\text{FM}}(x, y) + f_{\text{FVM}}(x, y))/2$.

NE adventitia edge pixels have the following properties: they must be above the NE intima; their intensity gradient must point upward; their distance to the FE intima has to be smaller than $\text{CD}_{\max}$. For each edge pixel satisfying these constraints, the value of the NE fuzzy adventitia score map is computed as

$$f_{\text{NE\_FAM}}(x, y) = f_{\text{FAM}}(x, y) e^{-z^2/2} \qquad (6)$$

where: (x, y) are the coordinates of this edge pixel; $z = \text{FAM}_{\max}/\sigma_{\text{FAM}}$; $\text{FAM}_{\max}$ is the maximum value of f_{FAM} between (x, y) and the NE intima contour, along the same column; σ_{FAM} is a scale parameter. This score favors edges with a stronger value of $f_{\text{FAM}}(x, y)$ and penalizes edges that have other plausible adventitia edges between them and the lumen. Figure 4 a) shows $f_{\text{NE\_FAM}}(x, y)$ computed for a ROI in the image of Fig. 1.

Finally, a DP algorithm processes $f_{\text{NE\_FAM}}(x, y)$ to estimate the NE adventitia (first white contour from the top in Fig. 4 c)), corresponding to the contour that maximizes a gain function like the one in equation (5), but setting $\psi(x_j, y_j) = f_{\text{NE\_FAM}}(x_j, y_j)$.

The FE fuzzy adventitia score map, $f_{\text{FE\_FAM}}(x, y)$, presented in Fig. 4 b), and the FE adventitia boundary, corresponding to the second white contour from the top in Fig. 4 c), are computed in a way similar to the one described for the NE adventitia. However, in this case $\psi(x_j, y_j) = f_{\text{FE\_FAM}}(x_j, y_j)$ and the following properties are considered for FE adventitia edge pixels: they must be below the FE intima; their intensity gradient must point downward; their distance to the NE intima has to be smaller than $\text{CD}_{\max}$.

3 Results

3.1 Parameter settings

The range of values observed in the dataset lead to the following settings: $\text{CD}_{\max} = 12.5$ mm and $L = 10$ pixels. Since the observed IMT can be almost as large as the lumen diameter, $\text{LD}_{\min}$ was set to 1 mm.

Table 1. Parameters that minimize the mean value of D_{mean} for the training image set and for the manual segmentations.

		σ_{FM}	σ_{FAM}	λ
Intima	NE	0.3	-	10
	FE	0.1	-	70
Adventitia	NE	-	0.30	110
	FE	-	0.45	90

A training phase, based on a subset of 20 images of the dataset, was necessary to estimate σ_{FM} (equation (4)), σ_{FAM} (equation (6)) and λ (equation (5)). The optimum values found for these parameters are given in Table 1.

The following results refer to the remaining subset of 30 images of the dataset. These images were not used in the training phase and correspond to a different set of patients.

3.2 Segmentation results

Several automatic segmentations of the intima-media region, delimited by the detected intima and adventitia contours, for the NE and FE carotid boundaries, are presented in the left column of Fig. 5. For comparison, the right column of this figure shows the corresponding results produced by the method introduced in [8] and [9]. The manual segmentations of the medical expert are also shown for reference.

The inter-method (manual versus automatic) errors were evaluated by the coefficient of variation, CV, computed for IMT_{mean}, the mean IMT of each segmented intima-media region. The coefficient of variation is determined by [3]

$$CV = 100\frac{se}{\overline{x}}\ \% \tag{7}$$

where $se = sd/\sqrt{2}$, $\overline{x}$ is the pooled mean and sd is the standard deviation of the differences in IMT_{mean} for the manual and the automatic segmentations of the same intima-media region. For the approach introduced in [8,9], the CV is 15.0% at NE boundaries and 21.5% at FE boundaries. For the new method the CV is 18.4% at NE boundaries and 6.4% at FE boundaries. The new approach does not show improvements at NE walls but it is much better at FE walls.

Using Matlab on a computer with an Intel Core 2 Duo processor at 2.13 GHz, the time required by the new approach to segment an image is in the range $[0.5, 2.1]$ s, with a mean of 0.8 s. For the previous approach, the median time is 18.9 s per intima boundary and 28.5 s per adventitia boundary.

4 Conclusion

A new method was introduced for the automatic segmentation of the CCA in B-mode images. It takes advantage of the ICOV edge detector and uses several discriminating features of the intima and adventitia boundaries.

The proposed method has a simpler implementation and requires much shorter processing times than the approach recently introduced in [8] and [9]. It is also robust, since it is able to segment both the NE and FE

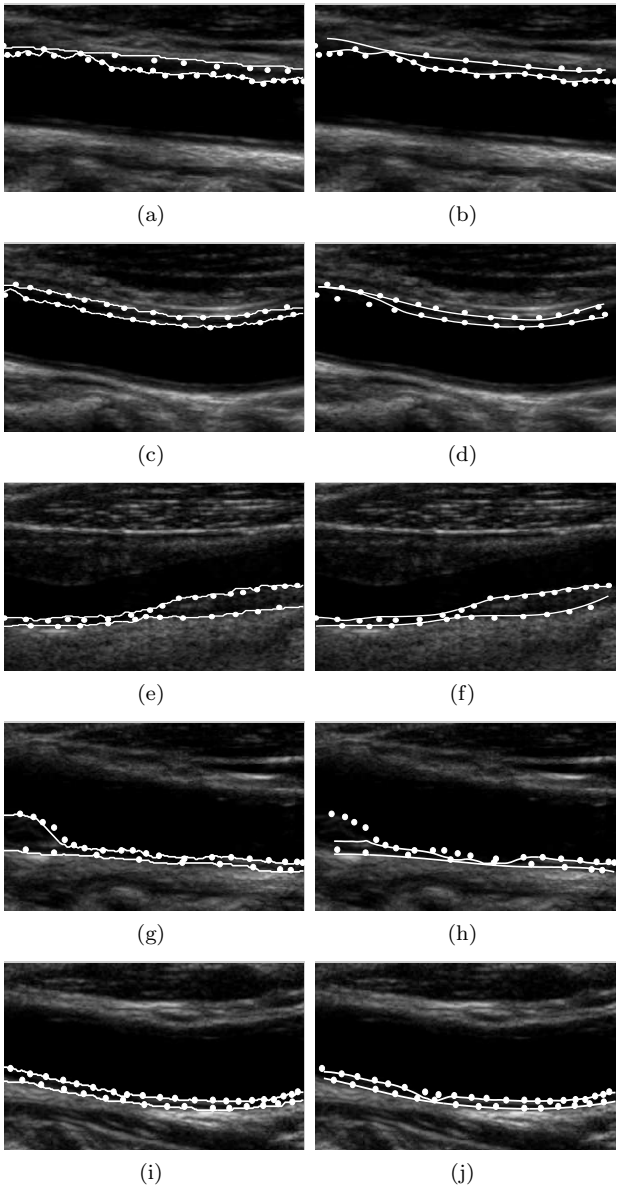

Figure 5. Examples of manual detections of the medical expert (white points) of the intima and adventitia boundaries, along with the corresponding automatic detections (white curves) produced by the proposed method (left column) and the approach introduced in [8, 9] (right column): a-d) NE wall; e-j) FE wall. Images e) to h) show two arteries with large class III plaques of different shapes.

boundaries in healthy and in atherosclerotic arteries, with a wide range of plaque types and sizes, as illustrated by the examples shown in Fig. 5 e) and g), without the help of manual initializations or corrections of the DP contours.

One drawback of the method is the need for a training phase. Although no restrictions were made to the scanning parameters, the images of our database were all acquired with the same scanner model. Therefore, a normalization of the image histogram may be required to avoid a new training of the method when the algorithm is applied to images acquired with different scanners.

The automatic results are similar to the manual ones, specially at the FE wall, where the visibility of the intima and adventitia boundaries is generally better. It is more difficult to detect NE boundaries than FE ones, even for medical experts. This problem is a consequence of the poorer visibility of NE boundaries, being more critical for the NE adventitia. The increased difficulty in detecting NE boundaries explains the preference for the FE wall in clinical practice, when it comes to IMT measurements. The high accuracy of the detections at FE walls and the short processing time suggest that the proposed method can be an effective aid in clinical practice for the IMT measurement at FE walls.

In a future work, the method should be submitted to a more comprising and detailed quantitative analysis, using manual segmentations performed by more than one medical expert and a larger dataset. The improvement of the discrimination between edges and the inclusion of more powerful classifiers are other important issues to be considered.

References

[1] D. Baldassarre, M. Amato, A. Bondioli, C. R. Sirtori, and E. Tremoli, "Carotid artery intima-media thickness measured by ultrasonography in normal clinical practice correlates well with atherosclerosis risk factors," *Stroke*, vol. 31, pp. 2426 – 2430, October 2000.

[2] A. Gee, R. Prager, G. Treece, and L. Berman, "Engineering a freehand 3D ultrasound system," *Pattern Recogn. Lett.*, vol. 24, no. 4-5, pp. 757–777, 2003.

[3] T. Gustavsson, Q. Liang, I. Wendelhag, and J. Wikstrand, "A dynamic programming procedure for automated ultrasonic measurement of the carotid artery," *Computers in Cardiology*, pp. 297–300, 1994.

[4] I. Wendelhag, Q. Liang, T. Gustavsson, and J. Wikstrand, "A new automated computerized analyzing system simplifies readings and reduces the variability in ultrasound measurement of intima-media thickness," *Stroke*, vol. 28, pp. 2195–2200, 1997.

[5] Q. Liang, I. Wendelhag, J. Wikstrand, and T. Gustavsson, "A multiscale dynamic programming procedure for boundary detection in ultrasound artery images," *IEEE Trans. Med. Imag.*, vol. 19, no. 2, pp. 127–142, 2000.

[6] D. Cheng, A. Schmidt-Trucksass, K. Cheng, and H. Burkhardt, "Using snakes to detect the intimal and adventitial layers of the common carotid artery wall in sonographic images," *Computer Methods and Programs in Biomedicine*, vol. 67, pp. 27–37, 2002.

[7] C. P. Loizou, C. S. Pattichis, M. Pantziaris, T. Tyllis, and A. Nicolaides, "Snakes based segmentation of the common carotid artery intima media," *Med. Bio. Eng. Comput.*, vol. 45, pp. 35–49, 2007.

[8] R. Rocha, A. Campilho, J. Silva, E. Azevedo, and R. Santos, "Segmentation of the carotid intima media region in B-mode images," *Image and Vision Computing*, vol. 28, pp. 614–625, 2010.

[9] ——, "Segmentation of ultrasound images of the carotid using RANSAC and cubic splines," *Computer Methods and Programs in Biomedicine*, vol. 101, pp. 94–106, 2011.

[10] Y. Yu and S. Acton, "Speckle reducing anisotropic diffusion," *IEEE Trans. Image Processing*, vol. 11, no. 11, pp. 1260–1270, 2002.

[11] ——, "Edge detection in ultrasound imagery using the instantaneous coefficient of variation," *IEEE Trans. Image Processing*, vol. 13, no. 12, pp. 1640–1655, 2004.

[12] M. Halenka, "Noninvasive measurement of early atherosclerosis by high-resolution B-mode ultrasonography," *Acta-Universitatis Palackianae Olomucensis Facultatis Medicae*, vol. 142, pp. 7–12, 1999.